Supporting information

Single-site carbon layer-based flexible interdigitated micro-supercapacitor: custom miniaturization and surface functional engineering

Mariyarathinam Vinoth Inbaraj, and Govindhan Maduraiveeran*

Materials Electrochemistry Laboratory, Department of Chemistry, SRM Institute of Science and Technology, Kattankulathur - 603 203, Chengalpattu, Tamil Nadu, India

**Corresponding Author: maduraig@srmist.edu.in & pgmadura@yahoo.co.in; Tel. Phone: 044- 2741 6268*

EXPERIMENTAL SECTION:

Materials:

Potassium hydroxide (KOH), Sodium nitrate ($NaNO_3$), and acetone were received from SRL Pvt. Ltd., Maharashtra, India. Nitric acid was purchased from RANKEM, Maharashtra, India. Ethanol received from Hayman, Witham, UK. Commercial carbon fiber microelectrodes, (diameter: ~300 μm) with a purity of 99.99% were acquired from Sigma Aldrich, USA. The carbon microfiber (CMF) underwent an ultrasonic treatment using a 1:1 ethanol-to-acetone ratio for a brief period after being repeatedly cleaned with deionized water. The CMF then reached 50 ^{0}C to fully dry. Following the pretreatment, the CMF is referred to as an electrode pristine-CMF electrode. All of the chemicals were analytical grade and were used straight without further purifications.

Electrochemical augmentation process for single-site carbon layers

The pretreated pristine CMF microelectrode with a geometrical surface area of ~0.096 cm^2 (a radius of ~150 μm and a height of ~10 mm). The precleaned pristine CMF electrode was immersed in 3.0 M KOH. The cyclic voltammograms (CV) of the CMF electrodes were recorded in the operating potential range, starting from -0.2 V to +0.8 V (vs. Ag/AgCl) at a

scan rate of 10.0 mV s^{-1} for various continuous cycles. The as-developed electrodes are designated as SSC-50, SSC-100, SSC-200, and SSC-350 for 50, 100, 200, and 350 cycles, respectively. For controlled studies, a similar electrochemical oxidation process was conducted in acid (1.0 M HNO_3) and neutral (1.0 M $NaNO_3$) electrolytes to perform the micro-supercapacitor (MSC) studies.

Fabrication of interdigitated micro-supercapacitor device

Primarily, to prepare the gel electrolyte, 1 g of polyvinyl alcohol (PVA) was mixed with 10 mL of deionized water. The above mixture was then heated to 60°C, and 10 ml of 3.0 M KOH was added slowly under vigorous stirring until it became clear. After coating the polyethylene sheet (1.0 cm^2) with the gel, the ~7 mm SSC-200|CMF and two current collectors (~15 mm) were immersed in it. After that, they were all left to gelatinize at room temperature (26 ±1 °C) for 3 min. Again, the electrodes and current collectors were dipped in gel electrolyte and assembled with the interdigitated shape with a space of ~2 mm on the sheet. They were then covered with gel electrolyte, which was then left to fix at room temperature for 24 h.

Characterization

The surface morphology and elemental composition were investigated using high-resolution scanning electron microscopy (HR-SEM, FEI QUANTA 200). Transmission electron microscopic (TEM) and high-resolution transmission electron microscopic (HRTEM) studies were conducted with a JEOL 2010F TEM. The functional groups were identified using FT-IR spectroscopy a SHIMADZU, IRTRACERR 100. To study the X-ray diffraction (XRD) patterns, a PAN analytical Xpert Pro diffractometer with a monochromatic Cu Kr (1.5406, 2.2 KW Max) filter was used. Raman spectroscopy experiments were carried out with a HORIBA, LabRam HR Evolution Resolution: 0.4 cm^{-1} (@ 532 nm). X-ray photoelectron spectroscopy

(XPS) (XPS-PHI Versa probe III) was used to investigate the chemical state and chemical composition analysis of the electrodes.

Electrochemical measurements:

Cyclic voltammetry (CV) was used to assess the electrochemical characteristics of the carbon fiber electrodes using the Metrohm Autolab B.V. workstation (AUT204). The electrochemical impedance spectroscopy (EIS), cycling stability test, and galvanostatic charged-discharge (GCD) methods were conducted with an OrigaLys multichannel system (Origaflex OGF500) workstation at the open-circuit potential without bias potential. Electrochemical experiments were conducted at room temperature in three different electrolyte mediums (1.0 M HNO_3, 1.0 M $NaNO_3$, and 3.0 M KOH). CV was performed at various scan rates, starting from 10 to 100 mV s^{-1}, and GCD was performed with current densities from 0.1 to 0.5 mA cm^{-2} and a potential from 0 to 0.5 V. The EIS measurement's frequency range and AC amplitude were set from 100 kHz to 10 mHz at an amplitude of 5 mV.

Calculation method

The electrochemical tests in the current investigation are therefore set by the area ratio parameters.[1,2] The areal capacitance and the areal energy and power densities suggest the properties of flexible AI-MSCs.[3–5] Eqn. (1) and (2) were used to compute the areal capacitance of single electrodes from GCD and CV[6], respectively, and the eqn. (3) computes the device's areal capacitance. Eqn. (4) and (5) were used to compute the areal energy and power densities[7,8].

$$\mathrm{A.\,C_{(Electrode)}} = \frac{2\mathrm{I} \times \Delta \mathrm{t}}{\Delta V} \qquad (1)$$

$$A.C_{(Electrode)} = \frac{\int IdV}{v \times A \times \Delta V} \qquad (2)$$

$$\mathrm{A.C_{(Device)}} = \frac{\mathrm{I} \times \Delta \mathrm{t}}{\Delta V} \qquad (3)$$

$$\mathrm{E_{(Device)}} = \frac{A.C_{(Device)} \times \Delta V^2}{2} \qquad (4)$$

$$P_{(Device)} = \frac{E_{(Device)}}{\Delta \mathrm{t}} \qquad (5)$$

Where A.C represents the areal capacitance; E and P mean the energy and power densities of the device; I represents the current density of charge and discharge; $\int IdV$ represents the absolute area; v represents the scan rate; ΔV represents the potential window; and Δt is the discharge time.

The electrochemical active surface area (ECSA) of the electrodes was calculated using the double layer capacitance (C_{dl}) and specific capacitance C_s (22 μF cm^{-2}) [9] using Eqn. 6.

$$ECSA = \frac{C_{dl}}{C_s} \qquad (6)$$

Additionally, using Eqn. (7), the roughness factor (RF) of the electrodes can be calculated using ECSA and geometrical surface area (GSA).

$$RF = \frac{ECSA}{GSA} \qquad (7)$$

The Coulombic efficiency (η) of the SSC-200|CMF and AI-MSCs was calculated from the GCD curve using the Eqn. (8). where t_c and t_d represent the charge and discharge times, respectively.

$$\eta = \frac{t_d}{t_c} \times 100\ \% \qquad (8)$$

$$i(V) = k_1 V + k_2 V^{0.5} \qquad (9)$$

The overall capacitive and diffusive contribution is evaluated by using the Dunn method equation (Eqn. (9)). *i*(V) is the total current measured at a particular voltage (V) in the CV, and (k_1V) is the capacitive contribution, and $k_2V^{0.5}$, is the diffusive contribution[10].

Table S1. Elemental values of the electronic equivalent circuit, the data extracted from Figs. 3(e) and S28 are listed.

Components	R_s **(Ω)**	R_p **(k Ω)**	C_{dl} **(μF)**
Pristine CMF	571.2	51.01	12.42
SSC-200|CMF	34.1	35.6	141.3
AI-MSCs	284.1	57.96	173.2

Table S2. Comparison of areal capacitance of the developed electrodes in this study.

Electrodes	**Activation Medium**	**Areal Capacitance (mF cm^{-2})**
SSC-50|CMF	KOH	13 @ 0.1 mA cm^{-2}
SSC-100|CMF	KOH	17.9 @ 0.1 mA cm^{-2}
SSC-200|CMF	KOH	30.5 @ 0.1 mA cm^{-2}
SSC-200|CMF	HNO_3	1.7 @ 0.1 mA cm^{-2}
SSC-200|CMF	$NaNO_3$	1.1 @ 0.1 mA cm^{-2}
SSC-350|CMF	KOH	25.4 @ 0.1 mA cm^{-2}
Symmetric AI-MSCs	KOH	2.5 @ 0.1 mA cm^{-2}
Symmetric AI-MSCs	KOH (Solid)	0.43 @ 0.3 mA cm^{-2}

Table S3. Comparison of the supercapacitance performance of the recent electrode materials.

S.No	Material	Areal Capacitance	Areal Energy density	Areal power density	Stability Cycles	Capacitance Retention	References
1	AC-PEDOT:PSS	29.5 mF cm^{-2}	1.12 $\mu Wh/cm^2$	0.32 mW/cm^2	5000	85.9 %	Ref[11]
2	Mxene@ PTC-12	30.2 mF cm^{-2}	1.04 $\mu Wh/cm^2$	30 $\mu W/cm^2$	10,000	95 %	Ref [12]
3	N, O- Co-doped carbon	39.8 µF cm^{-2}	0.017 $\mu Wh/cm^2$	0.056 mW/cm^2	50,000	98 %	Ref[13]
4	PEDOT:PSS/Ketjenblack holey nanosheets	3.0 mF cm^{-2}	-	-	5000	80.4 %	Ref [14]
5	rGO/MXene and PEDOT:PSS	0.90 mF cm^{-2}	0.28 $\mu Wh/cm^2$	-	-	-	Ref [15]
6	Pseudo -Plastic Ox-SWCNT	0.1 mF cm^{-2}	0.51 $\mu Wh/cm^2$	0.59 mW cm^{-2}	10,000	85%	Ref [16]
7	PMo_{12}-modified SWCNTs	10.2 mF cm^{-2}	0.71 $\mu Wh/cm^2$	7 µW cm^{-2}	25,000	98.9%	Ref [17]
8	EG/CNT/AgNW	21.6 mF cm^{-2}	2 µWh cm−2	2.5 mW cm^{-2}	2000	93.1%	Ref [18]
9	Graphene - CNT (G-CNT) composite ink	9.81 mF cm^{-2}	1.36 µWh cm^{-2}	0.02 mW cm^{-2}	10,000	95.5%	Ref [19]
10	**AI-MSCs**	**30.5 mF cm^{-2}**	**0.015 $\mu Wh/cm^2$**	**11.0 µW cm^2**	**50,000**	**125 %**	**This Work**

PEDOT:PSS -Poly (3,4-ethylenedioxythiophene) polystyrene sulfonate; Ox-SWCNT - Oxidized single-walled carbon nanotubes; rGO – Reduced graphene oxide; PMo - Phosphomolybdic acid.

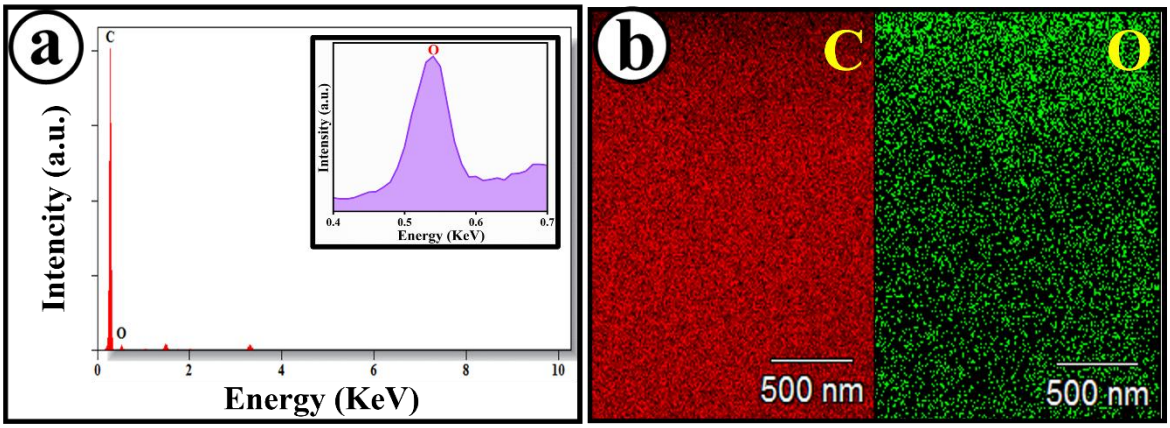

Fig. S1. EDX spectra (a) and elemental mapping (b) of the augmented SSC-200|CMF electrode.

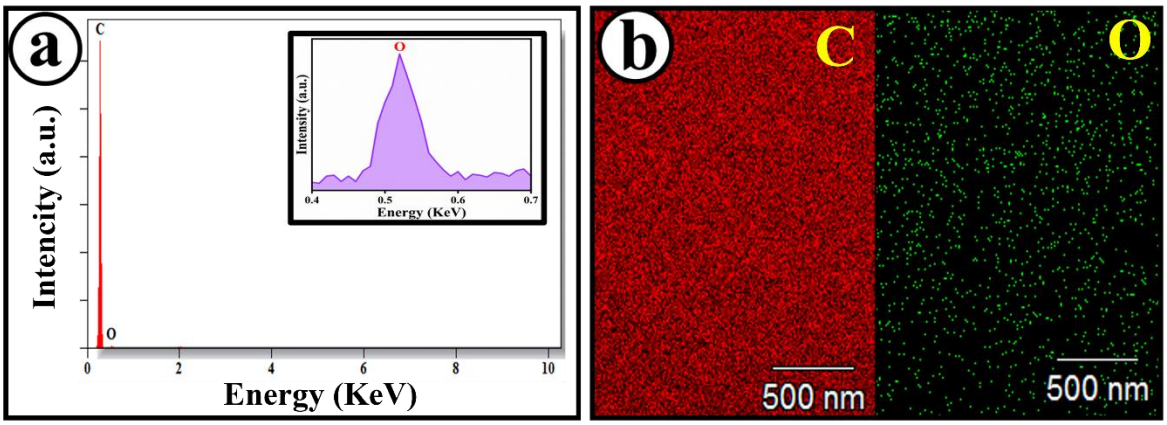

Fig. S2. EDX spectra (a) and elemental mapping (b) of the pristine CMF electrode.

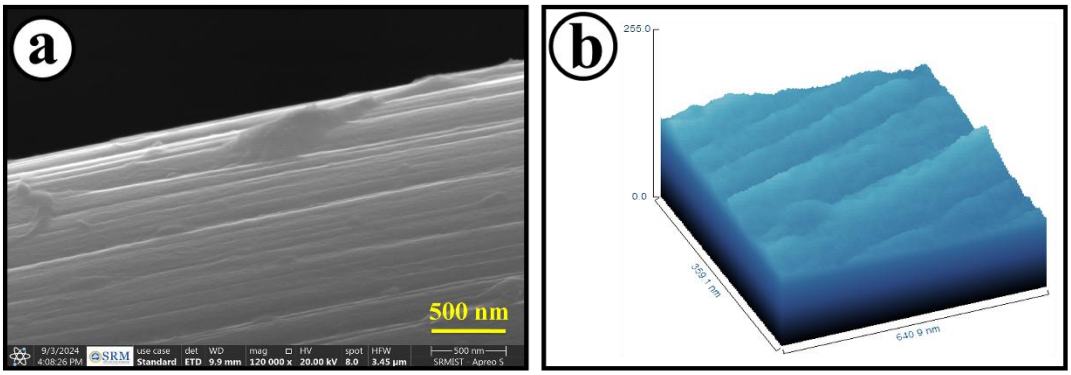

Fig. S3. FESEM image (a) and the surface plot (b) of the SSC-50|CMF electrode.

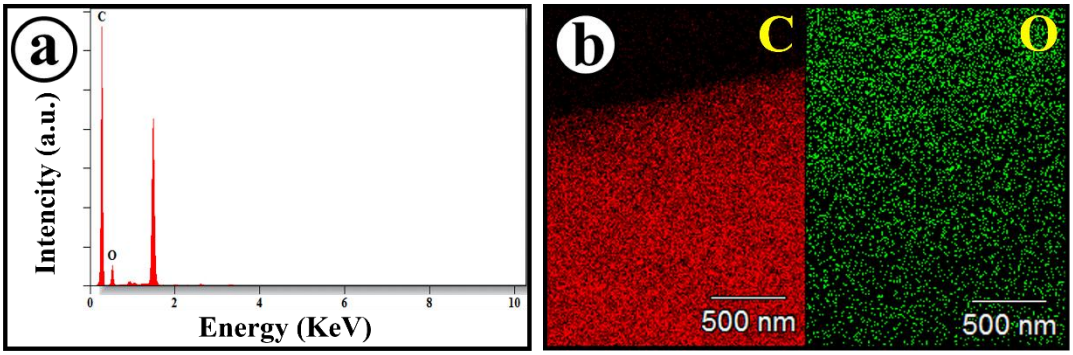

Fig. S4. EDX spectra (a) and elemental mapping (b) of the SSC-50|CMF electrode.

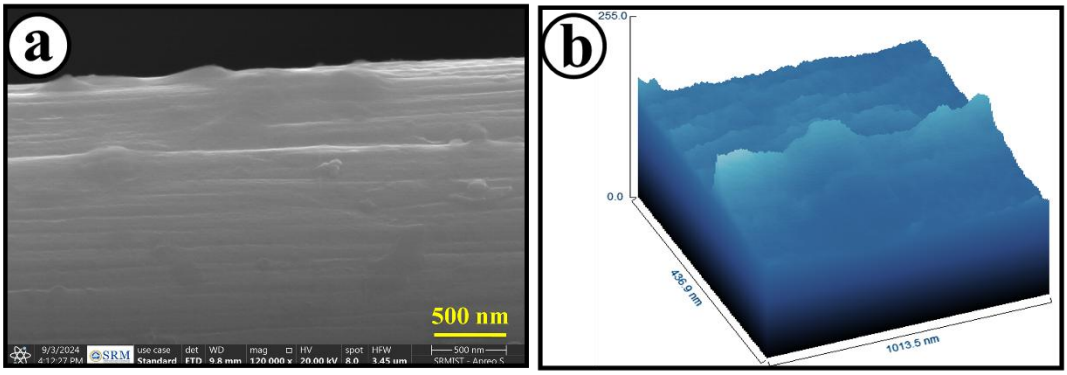

Fig. S5. FESEM image (a) and the surface plot (b) of the SSC-100|CMF electrode.

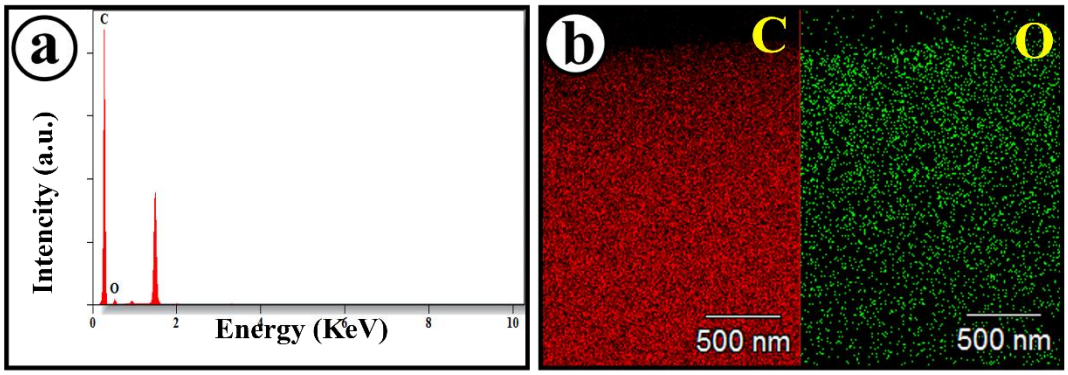

Fig. S6. EDX spectra (a) and elemental mapping (b) of the SSC-100|CMF electrode.

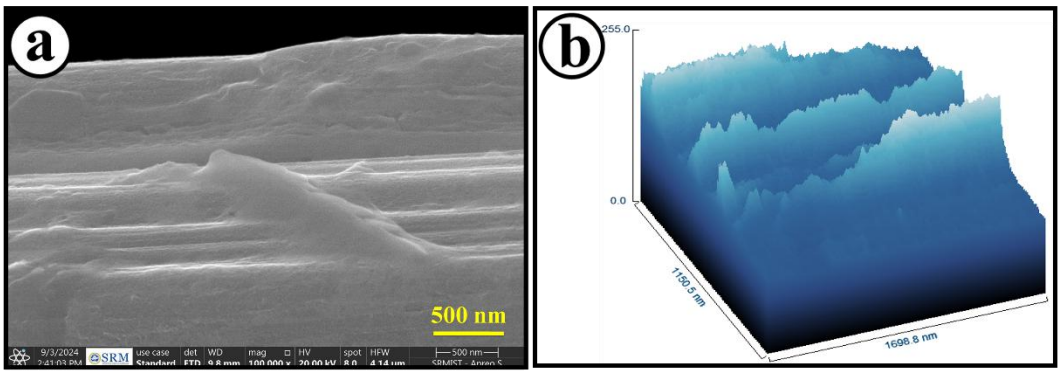

Fig. S7. FESEM image (a) and the surface plot (b) of the SSC-350|CMF electrode.

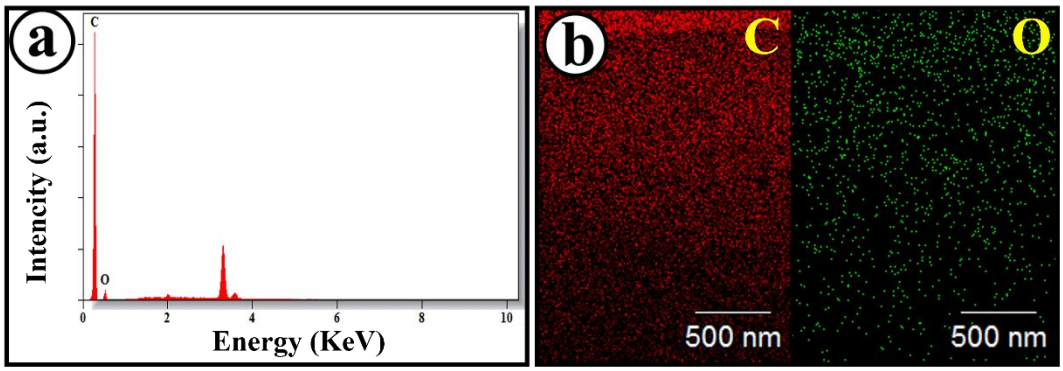

Fig. S8. EDX spectra (a) and elemental mapping (b) of the SSC-350|CMF electrode.

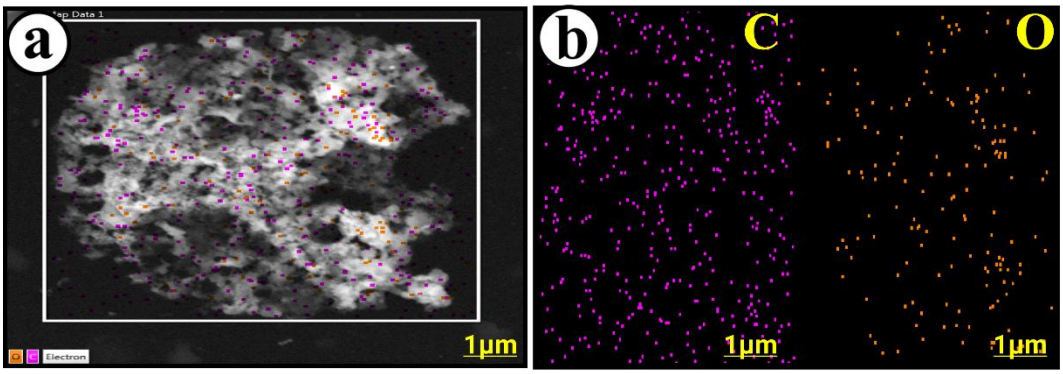

Fig. S9. HRTEM image (a) and elemental mapping (b) of the SSC-200|CMF electrode.

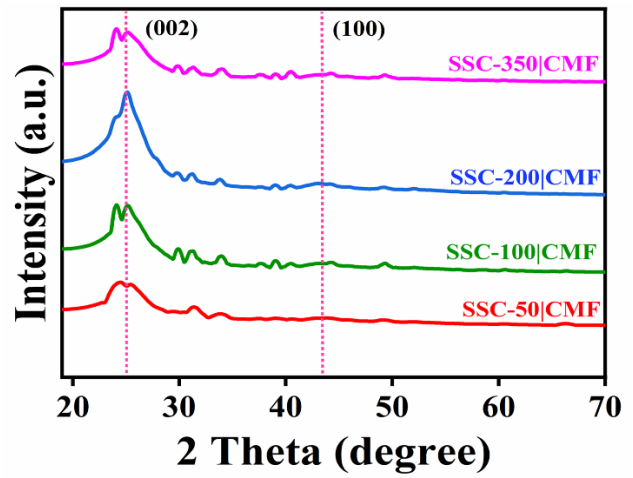

Fig. S10. XRD pattern of the developed various SSC|CMF.

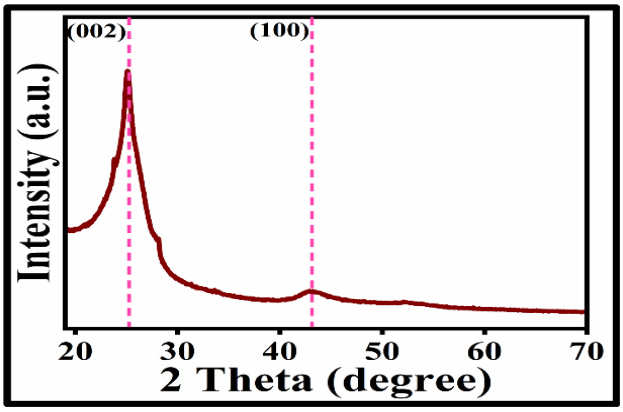

Fig. S11. XRD pattern of the pristine CMF electrode.

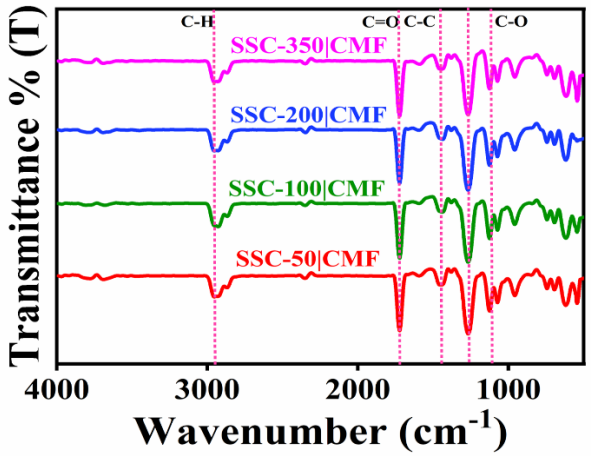

Fig. S12. FTIR spectra of the developed various SSC|CMF.

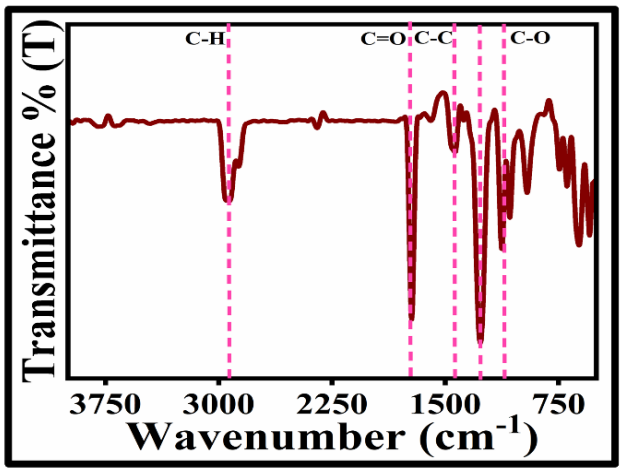

Fig. S13. FTIR spectra of the pristine CMF electrode.

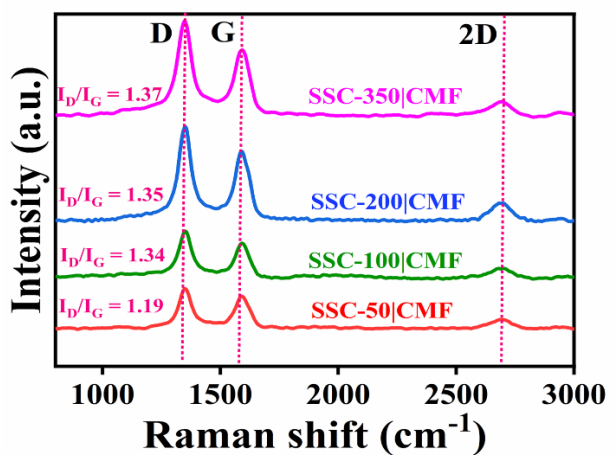

Fig. S14. Raman spectrum for the developed various SSC|CMF.

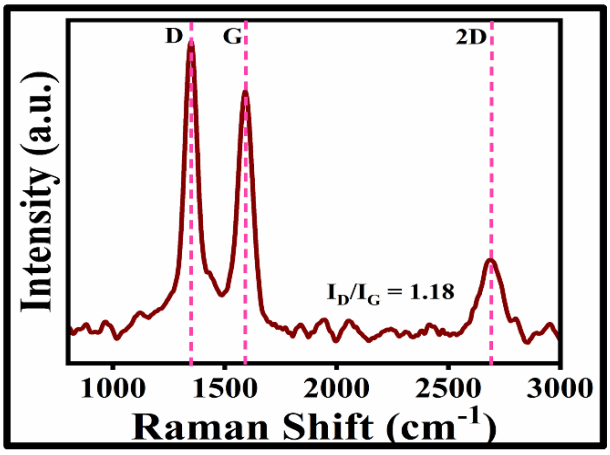

Fig. S15. Raman spectrum for the pristine CMF electrode.

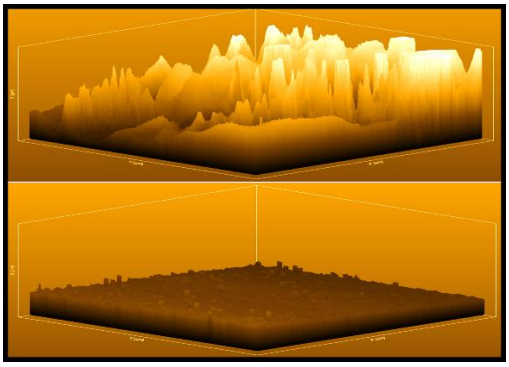

Fig. S16. Surface plots of SSC-200|CMF electrode (top) and pristine CMF electrode (bottom), derived from Raman spectra.

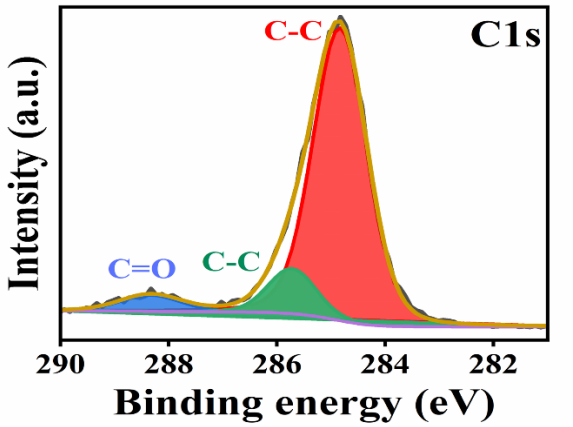

Fig. S17. High-resolution XPS spectra of C 1s for the SSC-200|CMF electrode.

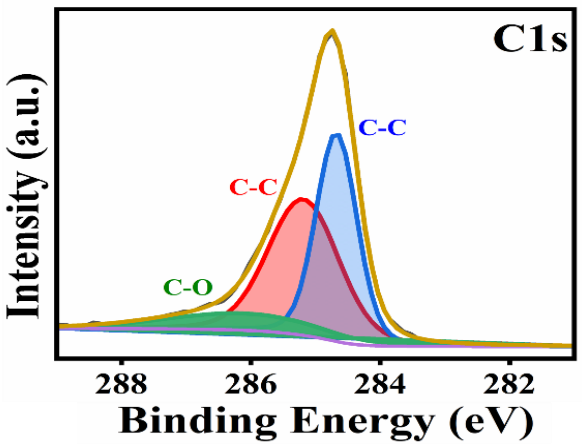

Fig. S18. XPS spectra (C1s) of the pristine CMF electrode.

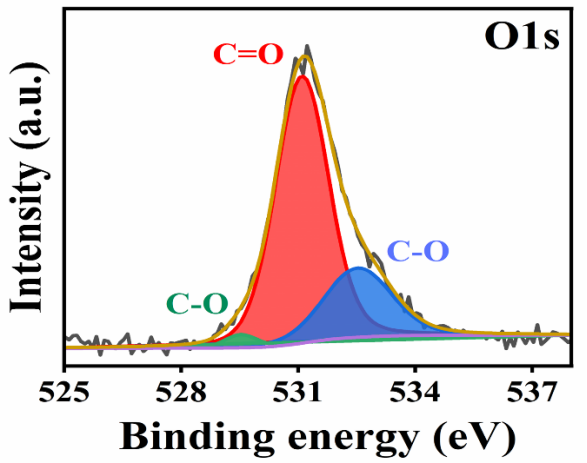

Fig. S19. High-resolution XPS spectra of O 1s for the SSC-200|CMF electrode.

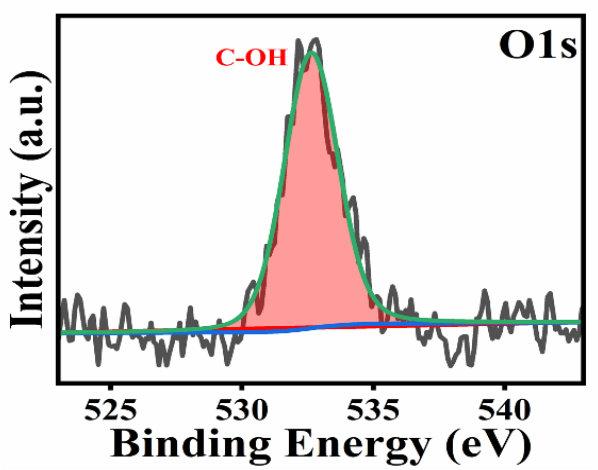

Fig. S20. XPS spectra (O1s) of the pristine CMF electrode.

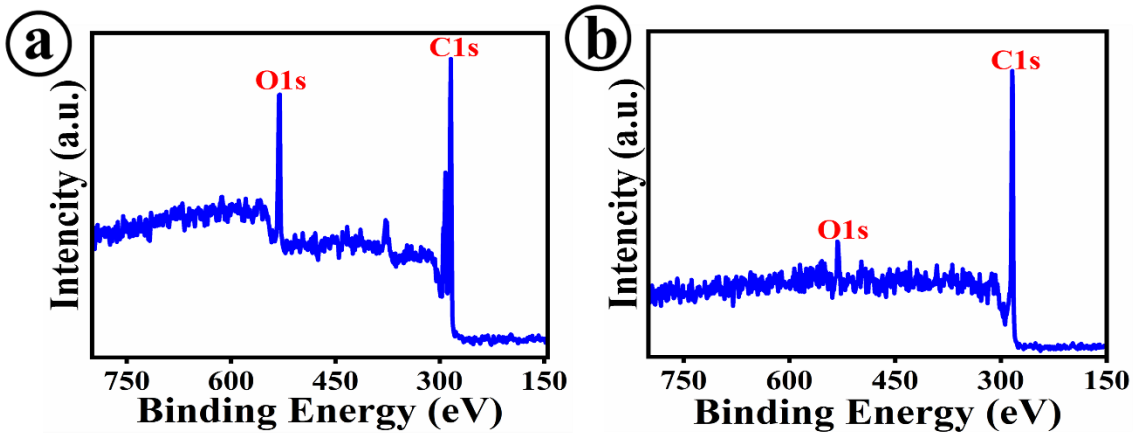

Fig. S21. XPS survey spectra of the pristine CMF (a) and SSC-200|CMF (b) electrodes.

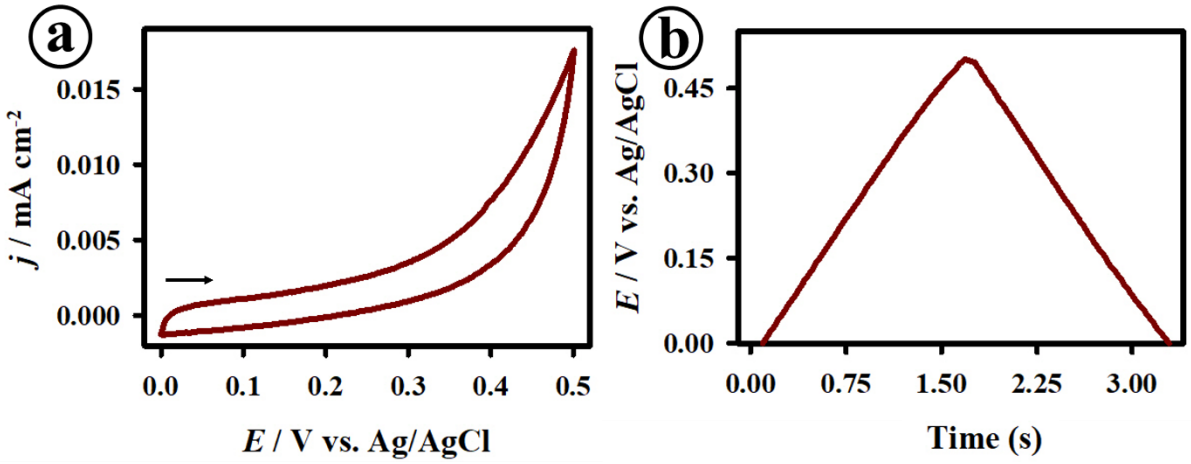

Fig. S22. CV curve at a scan rate of 100 mV s^{-1} (a) and GCD curve at 0.1 mA cm^{-2} current density (b) of the pristine CMF electrodes recorded in 3.0 M KOH.

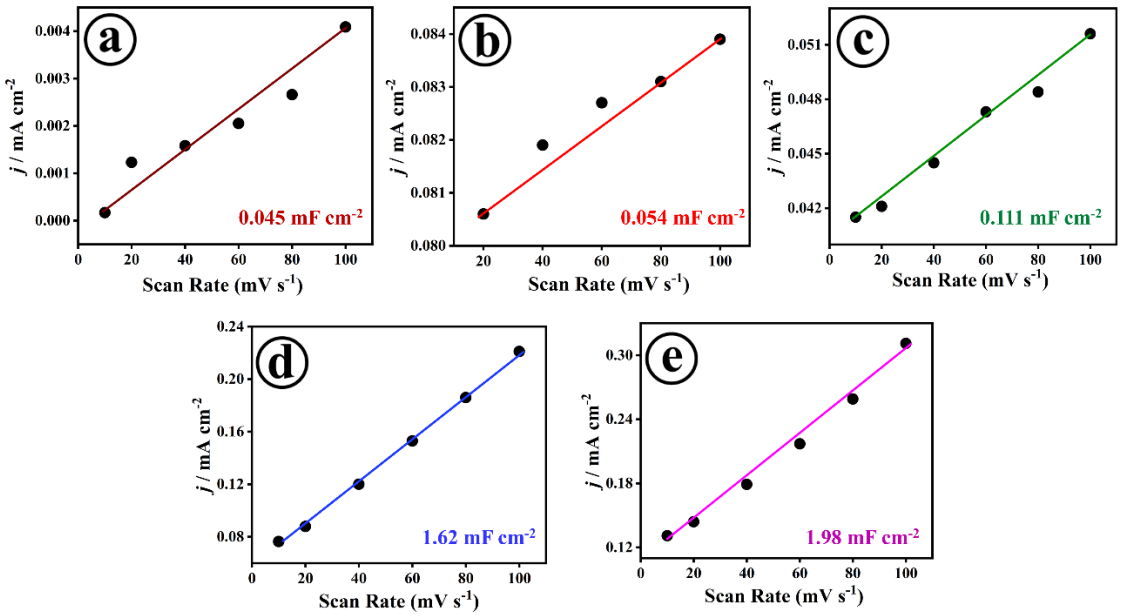

Fig. S23. ECSA plots of the pristine CMF (a), SSC-50|CMF (b), SSC-100|CMF (c), SSC-200|CMF (d) and SSC-350|CMF electrodes (e).

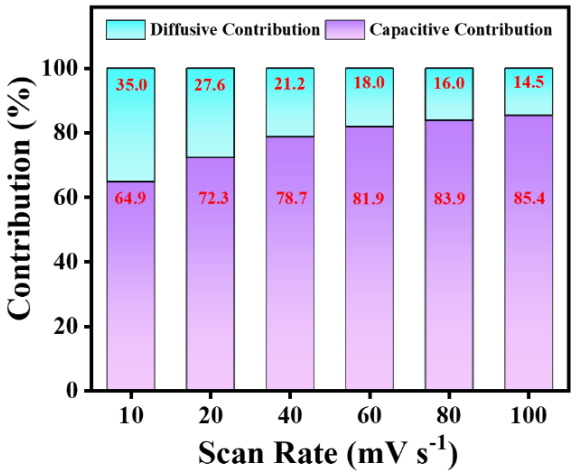

Fig. S24. Diffusive and capacitive contribution in percentage (%) of the SSC-200|CMF electrode.

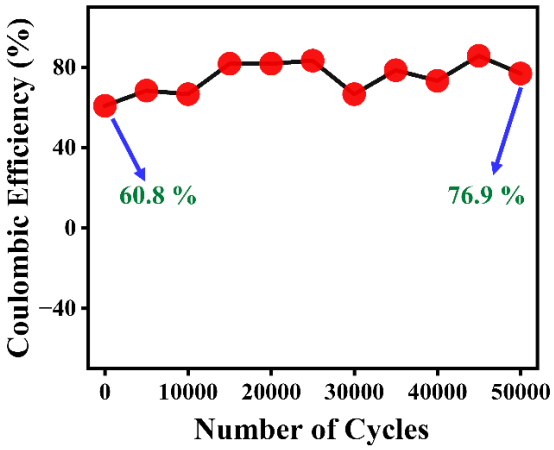

Fig. S25. Coulombic efficiency plots of the SSC-200|CMF electrode.

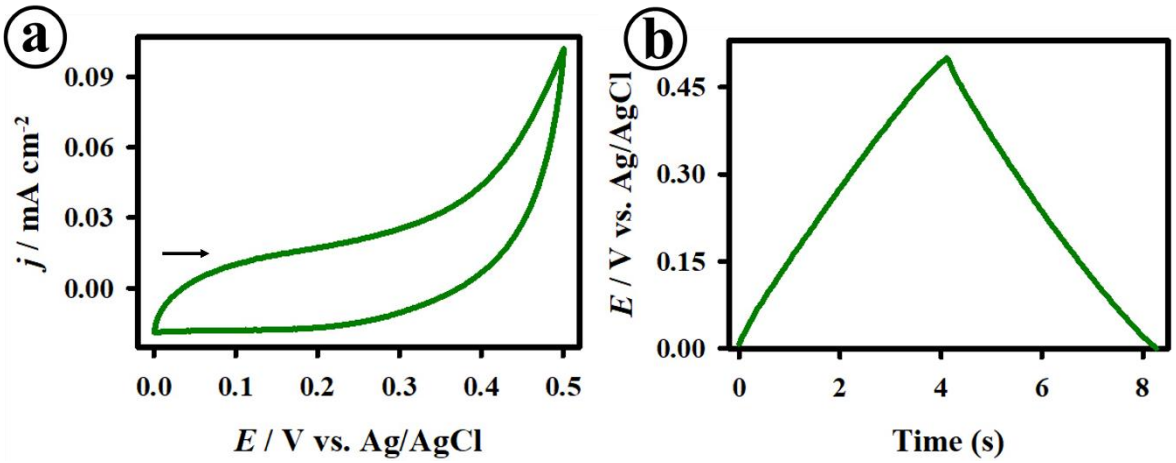

Fig. S26. CV curve (a) and GCD curve (b) recorded at the current density of 0.1 mA cm^{-2} at the SSC-200|CMF electrode in 1.0 M $NaNO_3$ at a scan rate of 100 mV s^{-1}.

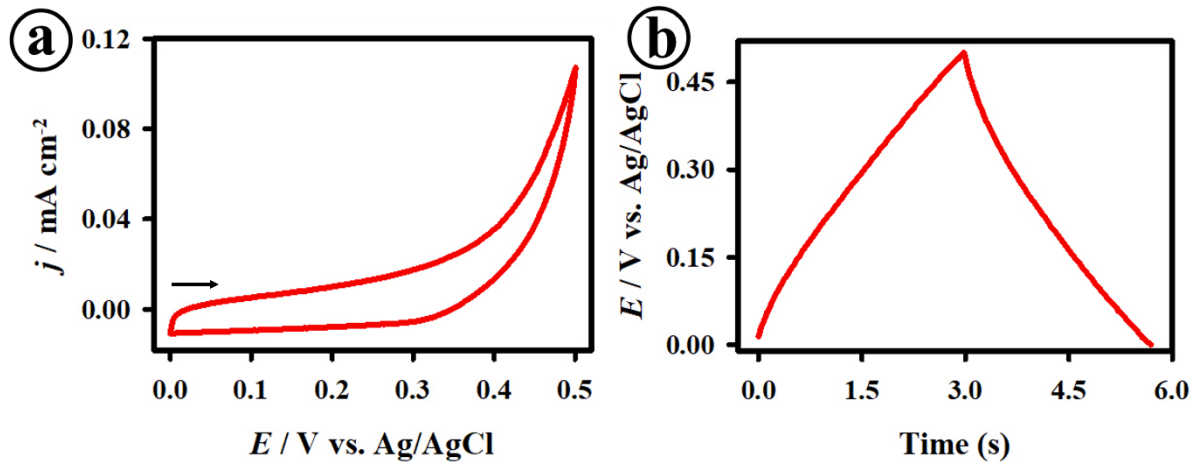

Fig. S27. CV curve (a) and GCD curve (b) recorded at the current density of 0.1 mA cm^{-2} at the SSC-200|CMF electrode in 1.0 M HNO_3 at a scan rate of 100 mV s^{-1}.

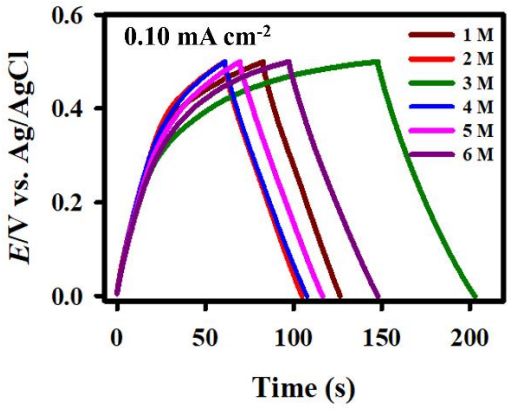

Fig. S28. GCD curves of the SSC-200|CMF electrodes recorded in different molar concentrations of KOH.

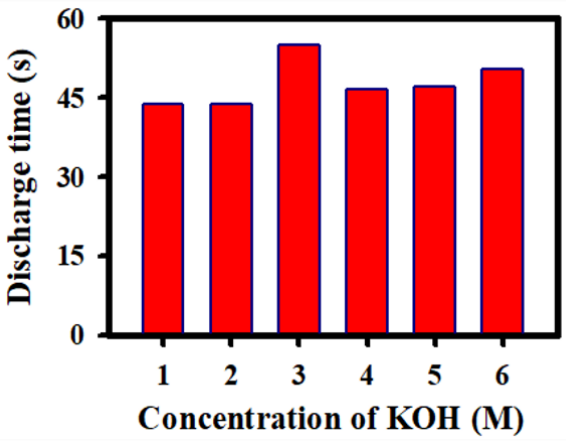

Fig. S29. Bar diagram for discharging time of the SSC-200|CMF electrodes with different molar concentrations.

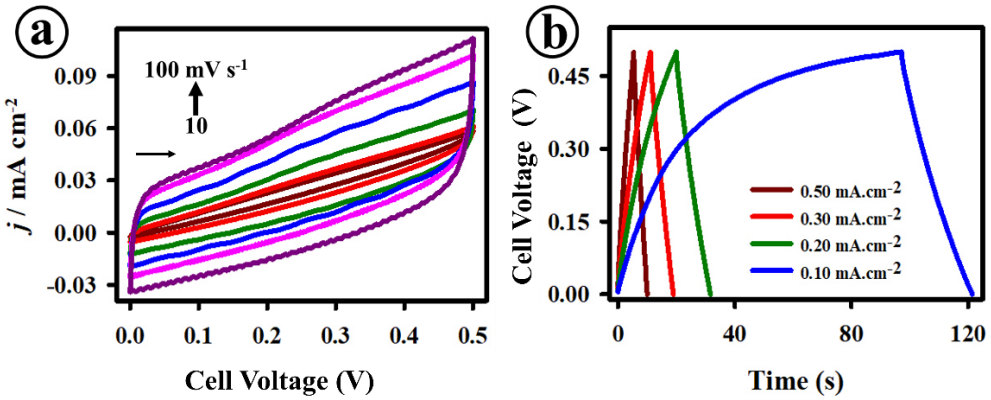

Fig. S30. CV (a) and GCD (b) curves of the SSC-200|CMF electrodes based on two electrode systems recorded in 3.0 M KOH.

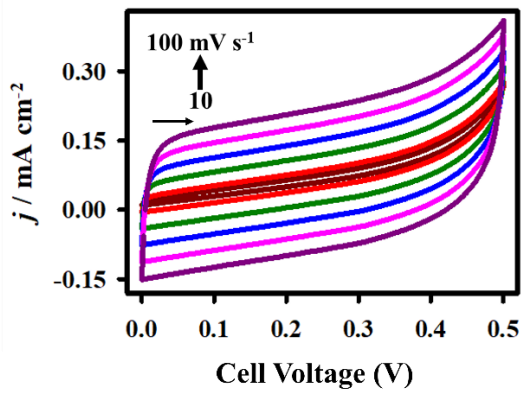

Fig. S31. CV curves of the symmetric interdigitated AI-MSCs.

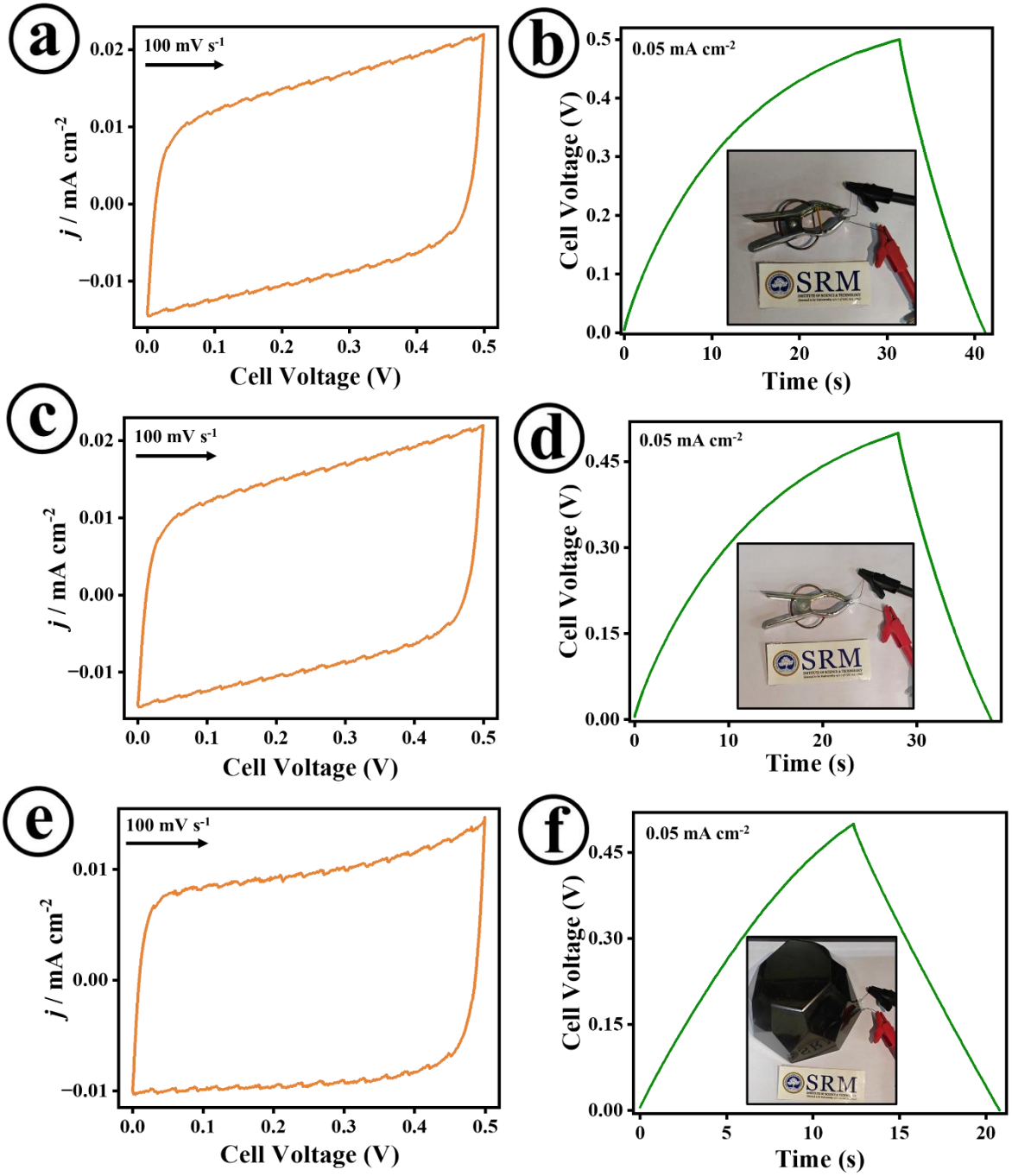

Fig. S32. CV (a) and GCD (b) curves with 50% folded AI-MSCs (Inset: Image proof of 50% folded AI-MSCs); CV (c) and GCD (d) curves with 100% folded AI-MSCs (Inset: Image proof of 100% folded AI-MSCs); CV (e) and GCD (f) curves of weight stressed AI-MSCs (Inset: Image proof of weight stressed AI-MSCs).

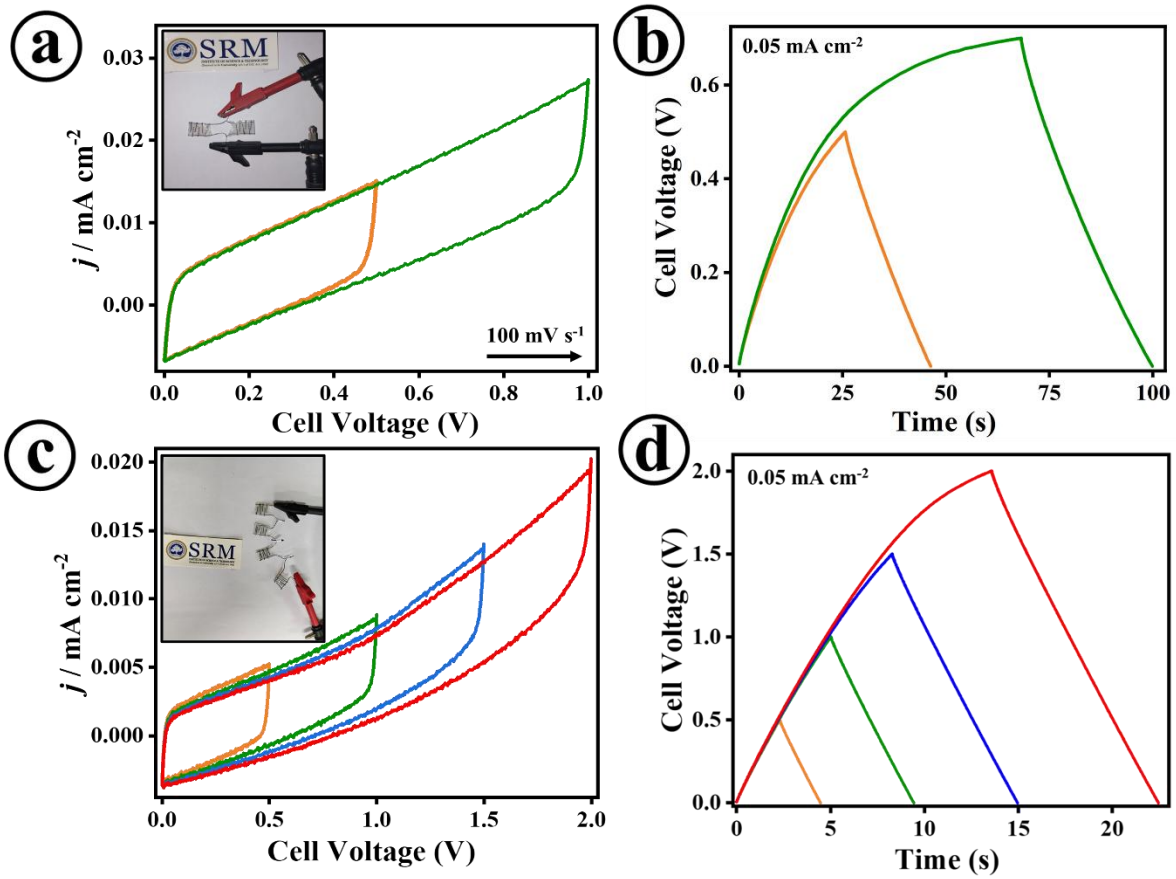

Fig. S33. CV (a) and GCD (b) curves of parallelly connected devices of AI-MSCs at different voltages (Inset of (a): Image proof of parallelly connected devices of A-MSCs), CV (c) and GCD (d) curves of serially connected devices of AI-MSCs at different voltages (Inset of (a): Image proof of serially connected devices of A-MSCs).

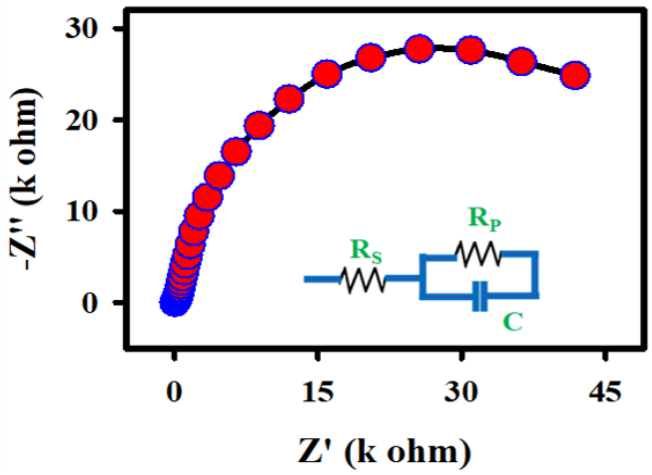

Fig. S34. EIS spectra of the symmetric AI-MSCs.

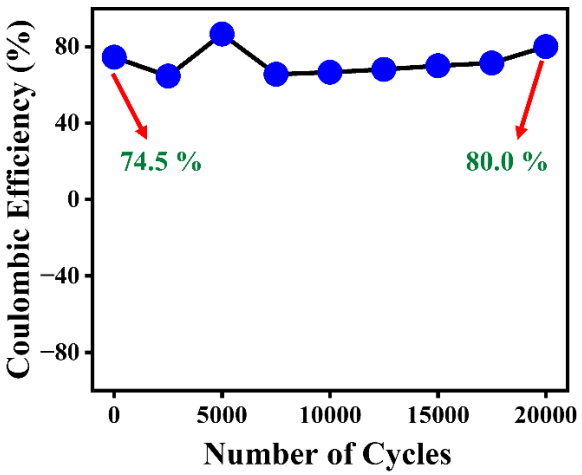

Fig. S35. Coulombic efficiency plots for the AI-MSCs device.

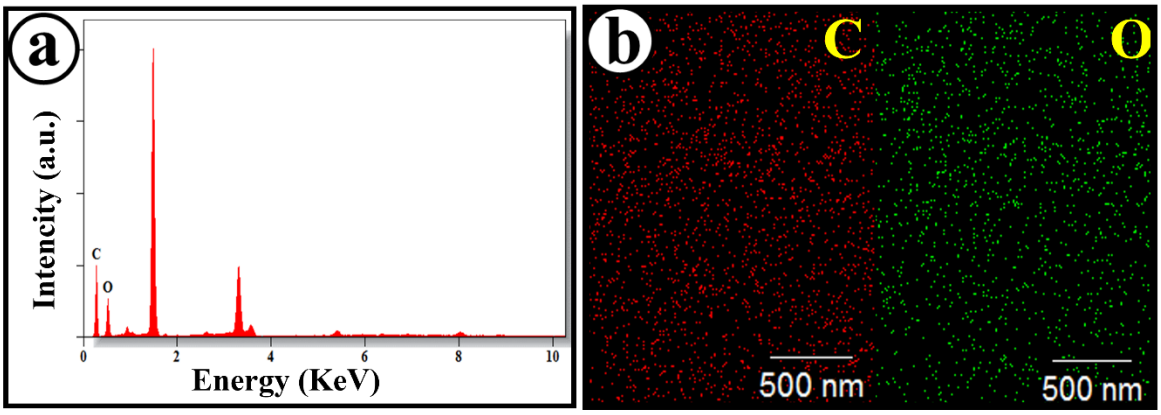

Fig. S36. EDX spectra (a) and elemental mapping (b) of the SSC-200|CMF after the stability.

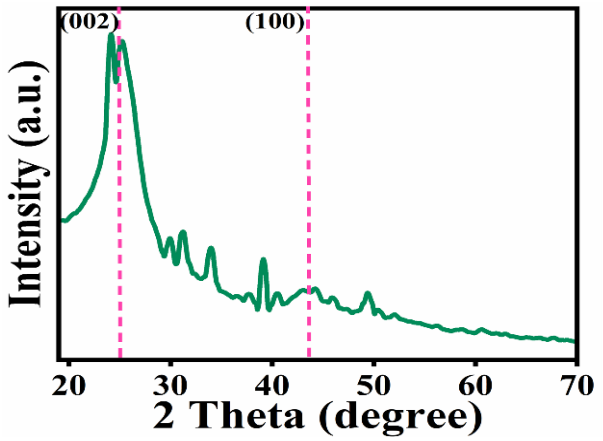

Fig. S37. XRD pattern of the SSC-200|CMF after the stability test.

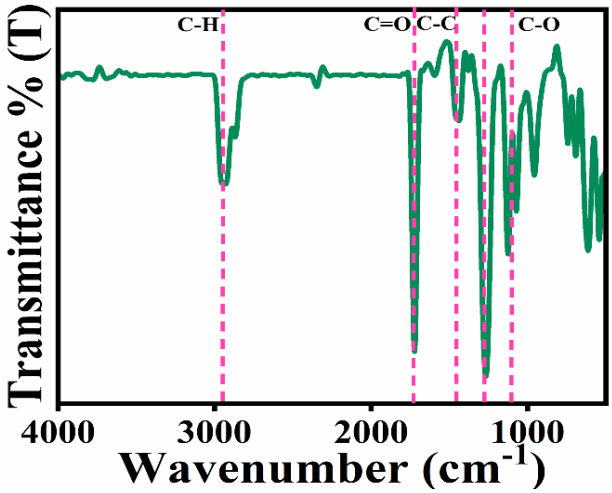

Fig. S38. FTIR spectra of the SSC-200|CMF electrode after the stability test.

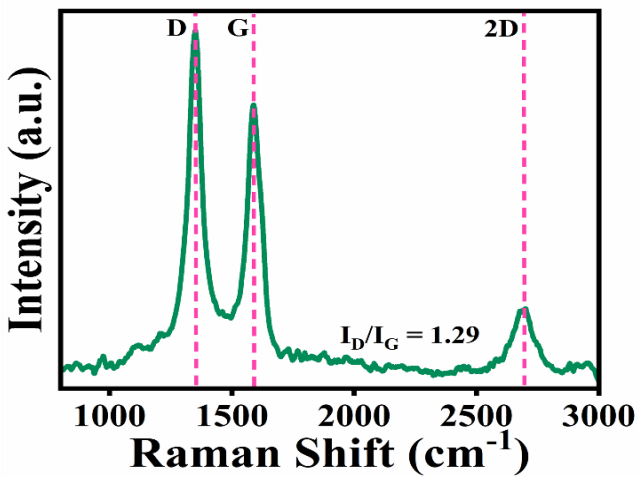

Fig. S39. Raman spectra of the SSC-200|CMF electrode after the stability test.

Reference

1 D. Li, S. Yang, X. Chen, W.-Y. Lai and W. Huang, *Adv. Funct. Mater.*, 2021, **31**, 2107484.

2 Y. Da, J. Liu, L. Zhou, X. Zhu, X. Chen, and L. Fu, *Adv. Mater.*, 2019, **31**, 1802793.

3 W. A. Haider, L. He, H. A. Mirza, M. Tahir, A. M. Khan, K. A. Owusu, W. Yang, Z. Wang and L. Mai, *RSC Adv.*, 2020, **10**, 18245–18251.

4 H. Li, J. Luo, S. Ding and J. Ding, *Nanoscale*, 2024, **16**, 14574–14588.

5 W. Zong, Y. Ouyang, Y.-E. Miao, T. Liu and F. Lai, *Chem. Commun.*, 2022, **58**, 2075–2095.

6 Y.-J. Gu, W. Wen and J.-M. Wu, *J. Mater. Chem. A*, 2018, **6**, 21078–21086.

7 A. Sharma, A. Patra, K. Namsheer, P. Mane, B. Chakraborty and C. S. Rout, *J. Mater. Sci.*, 2021, **56**, 20008–20025.

8 N. Kurra, C. Xia, M. N. Hedhili and H. N. Alshareef, *Chem. Commun.*, 2015, **51**, 10494–10497.

9 C. C. L. McCrory, S. Jung, J. C. Peters and T. F. Jaramillo, *J. Am. Chem. Soc.*, 2013, **135**, 16977–16987.

10 C. Gunasekaran, G. Shanmugam, S. Sreedhar and M. Venkatesan, *Electrochim. Acta*, 2025, **516**, 145725.

11 Y. Fan, T. Wang, R. Asrosa, B. Li, N. Naresh, X. Liu, S. Guan, R. Li, M. Wang, I. P. Parkin and B. D. Boruah, *Chem. Eng. J.*, 2024, **488**, 150672.

12 G. Zhu, Y. Hou, J. Lu, H. Zhang, Z. Zhuang, M. M. Baig, M. Z. Khan, M. A. Akram, S. Dong, P. Liu, X. Ge and Y. Zhang, *J. Mater. Chem. A*, 2023, **11**, 25422–25428.

13 F. Wei, X. He, L. Ma, H. Zhang, N. Xiao and J. Qiu, *Nano-Micro Lett.*, 2020, **12**, 82.

14 M. Zhao, Y. Qin, X. Wang, L. Wang, Q. Jin, M. Song, X. Wang and L. Qu, *Adv. Funct. Mater.*, 2024, **34**, 2313495.

15 L. Wang, L. Zhao, M. Song, L. Xie, X. Wang, X. Li, Y. Huang, M. Wei, Q. Jin, X. Meng and Y. Zhao, *J. Energy Chem.*, 2023, **78**, 158–168.

16 A. Jo, S. Chung, P. K. Kim, J.-W. Lee, H. J. Lee, H. J. Yang, T. Ha, J. Kim, Y. J. Lee, H. J. Jeong, S. H. Seo, S. Y. Jeong, G.-W. Lee, K.-J. Baeg, J. T. Han and J. H. Park, *ACS Appl. Energy Mater.*, 2021, **4**, 13666–13675.

17 H. Dong, J. Cao, Y. Ding, S. Wei, Z. Guo, L. Zhang, X. Zhou, Y. Liao, Q. Zhang and Z.-S. Wu, *Chem. Eng. J.*, 2024, **495**, 153509.

18 L. Liu, J. Lu, X. Long, R. Zhou, Y. Liu, Y. Wu and K. Yan, *Sci. China Technol. Sci.*, 2021, **64**, 1065–1073.

19 Y. Wang, Y. Zhang, G. Wang, X. Shi, Y. Qiao, J. Liu, H. Liu, A. Ganesh and L. Li, *Adv. Funct. Mater.*, 2020, **30**, 1907284.